Quaternary Research (2022), **105**, 37–48
doi:10.1017/qua.2021.28

Research Article

Sea surface temperature seasonality in the northern South China Sea during the middle Holocene derived from high resolution Sr/Ca ratios of *Tridacna* shells

Pengchao Zhou[a,b], Hong Yan[b,c,d*], Ge Shi[b], Chengcheng Liu[b], Fan Luo[e], Tao Han[b], Guozhen Wang[b], Hanfeng Wen[b], Nanyu Zhao[b], John Dodson[b], Yue Li[b] and Weijian Zhou[a,b,c]

[a]Interdisciplinary Research Center of Earth Science Frontier (IRCESF), Beijing Normal University, Beijing 100875, China; [b]State Key Laboratory of Loess and Quaternary Geology, Institute of Earth Environment, Chinese Academy of Sciences, Xi'an 710061, China; [c]CAS Center for Excellence in Quaternary Science and Global Change, Xi'an 710061, China; [d]Institute of Global Environmental Change, Xi'an Jiaotong University, Xi'an 710049, China and [e]Xi'an Institute for Innovative Earth Environment Research, Xi'an 710061, China

Abstract

Seasonal climate variability is an important component of Earth's climate system, and has a significant impact on ecosystems and social systems. However, the temporal resolution of most proxy-based paleoclimate records is limiting to fully understand the past seasonal changes. Here, we used high-precision monthly resolution Sr/Ca records of three *Tridacna squamosa* specimens from the northern South China Sea (SCS) to reconstruct the sea surface temperature (SST) seasonality during three time periods from the middle Holocene. The results suggested that SST seasonality in the northern SCS during the middle Holocene (3.21 ± 0.98°C) was smaller than that for recent decades (AD 1994–2004, 4.32 ± 0.59°C). Analysis of modern instrumental data showed that the SST seasonality in the northern SCS was dominated by the winter SST, which was deeply influenced by the intensity of East Asian winter monsoon (EAWM). A strong EAWM usually resulted in cooler winter SST and a larger SST seasonality in the northern SCS. The reconstructed Holocene EAWM records showed that the EAWM strengthened from the middle to late Holocene, which was seen in our reconstruction of less SST seasonality changes during the middle Holocene in the northern SCS. This study highlighted that the Sr/Ca ratios from *Tridacna* shells can be used as a potential high-resolution indicator of past seasonal climate changes.

Keywords: *Tridacna* shells, Seasonality, Sr/Ca, SST, Northern SCS, Middle Holocene, EAWM

(Received 14 December 2020; accepted 7 April 2021)

INTRODUCTION

Seasonal changes in climate, such as temperature seasonality (temperature contrast between summer and winter) and extreme seasonal climate events, have important impacts on natural and human systems (Andreasson and Schmitz, 2000; Wanamaker et al., 2011; Yan et al., 2015; Winter et al., 2020). Therefore, understanding the dynamics of the seasonal climate changes and predicting its future trends under expected future global warming should be one of the most important priorities in the climate sciences. However, the time span of high-resolution modern instrumental data is usually less than two hundred years, limiting our understanding of seasonal climate variations within the long-term climate background.

Paleoclimate proxy records, such as ice cores (Dansgaard et al., 1993; Petit et al., 1999), stalagmites (Polyak et al., 2001; Cheng et al., 2018), loess (An et al., 1991), lake sediments (Eawag et al., 1992; Chen et al., 2020), and tree rings (Fritts et al., 1979; Roig et al., 2001; Tian et al., 2007; Zaw et al., 2020), are important supplements for modern instrumental data, but most of these proxies cannot be used to study past seasonal climate changes because of their relatively low temporal resolution. Thus, developing high-resolution paleoclimate records, which can capture full seasonal cycles, are essential for us to reconstruct and understand past seasonal climate changes at a level that we need for mitigation and adaptability.

Marine biogenic carbonates, such as those found in corals and some bivalves (e.g., *Tridacnidae* spp., *Arctic islandica*, *Patella vulgata*, *Spisula solidissima*), have proven capable for reconstructing past seasonal climate variability because of their rapid growth rates and clear annual growth bands (e.g., Arthur et al., 1983; Schöne et al., 2005; Yu et al., 2005a; García-Escárzaga et al., 2018; Deng et al., 2019; Yan et al., 2020). Proxies that have been applied to reconstruct past sea surface temperatures (SST), sea surface salinity (SSS) and precipitation at a monthly resolution include geochemistry using elemental ratios and isotopes (e.g., Sr/Ca, Mg/Ca, $\delta^{18}O$, $\delta^{13}C$) (e.g., Yu et al., 2005b; Versteegh et al., 2010; Butler et al., 2011; Gorman et al., 2012; Bolton et al., 2014; Brocas et al., 2018).

Tridacna spp. may live over 100 years, and their shells are the largest bivalve shells in the world, measuring up to 1 m in

*Corresponding author: E-mail address: <yanhong@ieecas.cn>

Cite this article: Zhou P *et al* (2022). Sea surface temperature seasonality in the northern South China Sea during the middle Holocene derived from high resolution Sr/Ca ratios of *Tridacna* shells. *Quaternary Research* **105**, 37–48. https://doi.org/10.1017/qua.2021.28

diameter. Since the Eocene (ca. 50 million years ago), *Tridacna* spp. has been a key component of coral reefs in the tropical Indian-Pacific Ocean (Rosewater, 1964). *Tridacna* shells are sedentary, record environments at a fixed point in space, and their fast-growing shells usually have clear and visible annual growth bands. Powder samples that record monthly growth can be obtained from the annual bands of *Tridacna* by using a micro mill. Therefore, *Tridacna* spp. can be used as an ideal material to reconstruct past seasonal climate changes (Aharon and Chappell, 1986; Watanabe et al., 2004; Yan et al., 2015; Liu et al., 2019; Shao et al., 2020; Yan et al., 2020).

Oxygen isotopes have been used extensively to reconstruct the ambient paleotemperature from *Tridacna* shell carbonates (Welsh et al., 2011; Driscoll et al., 2014; Ayling et al., 2015; Yan et al., 2017; Hu et al., 2020; Shao et al., 2020). However, due to the simultaneous influence of SST and oxygen isotope composition of the surrounding seawater, there can be a relatively large uncertainty factor in reconstructing the past SST if the $\delta^{18}O$ content of ancient seawater is unknown (Aharon, 1983, 1991; Aharon and Chappell, 1986; Watanabe and Oba, 1999).

Because of the successful application of Sr/Ca thermometers in corals (Beck et al., 1992; McCulloch et al., 1996; Alibert and McCulloch, 1997), the Sr/Ca in *Tridacna* spp. has also been studied in recent years (Elliot et al., 2009; Batenburg et al., 2011; Yan et al., 2013, 2014a, 2014b, 2015). Based on the results of laser-ablation inductively coupled plasma mass-spectrometry (LA-ICP-MS; Elliot et al., 2009; Batenburg et al., 2011), early studies did not identify any significant correlation between monthly Sr/Ca of *Tridacna* spp. and SST. Subsequently, Yan et al. (2013, 2014a) determined the Sr/Ca of *Tridacna* spp. using inductively coupled plasma optical-emission spectrometry (ICP-OES), and found that the Sr/Ca profiles of *Tridacna* shells from the South China Sea (SCS) had obvious seasonal cycles and were significantly correlated with local SST. Thus, these studies showed that the Sr/Ca of *Tridacna* spp. had the potential to be used to reconstruct seasonal changes in SST.

The South China Sea is located at ~110°E to ~120°E, and ~5°N to ~20°N, between the eastern Indian Ocean and the western Pacific Ocean. As the largest semi-enclosed marginal sea in the northwest Pacific Ocean, climate in the SCS is controlled by the Asian monsoon on seasonal timescales and by El Niño-Southern Oscillation (ENSO) variability on inter-annual timescale (Sun et al., 2005; Wei et al., 2007; Wang and He., 2012; Kim et al., 2017). Therefore, high-resolution climate records derived from *Tridacna* spp. in the SCS have the potential to provide perspectives on the climate interactions between the mid-high latitudes and the tropics.

The middle Holocene (8000 to 3000 yr BP) has been proposed as a natural warm period in the history of Earth's climate by many studies (e.g., Chen et al., 2003; Ma et al., 2004; Ren et al., 2021). High-resolution climate records during the middle Holocene can help us understand the dynamics of seasonal climate changes and aid in predicting future climate trends under expected global warming. In this study, monthly Sr/Ca ratios from three middle Holocene *Tridacna squamosa* specimens from the North Reef of the northern SCS, with life spans of 34, 36, and 53 years, respectively, were determined. These high-resolution Sr/Ca data were used to reconstruct the middle Holocene SST seasonality changes in the northern SCS, and we discussed their relationship with regional and global climate changes below.

MATERIALS AND METHODS

Regional setting

The South China Sea, one of the three major marginal seas of China, is a semi-enclosed sea with a northeast-southwest directional trend, encompassing an area of ~3.5 million km^2 (Fig. 1a). The SCS

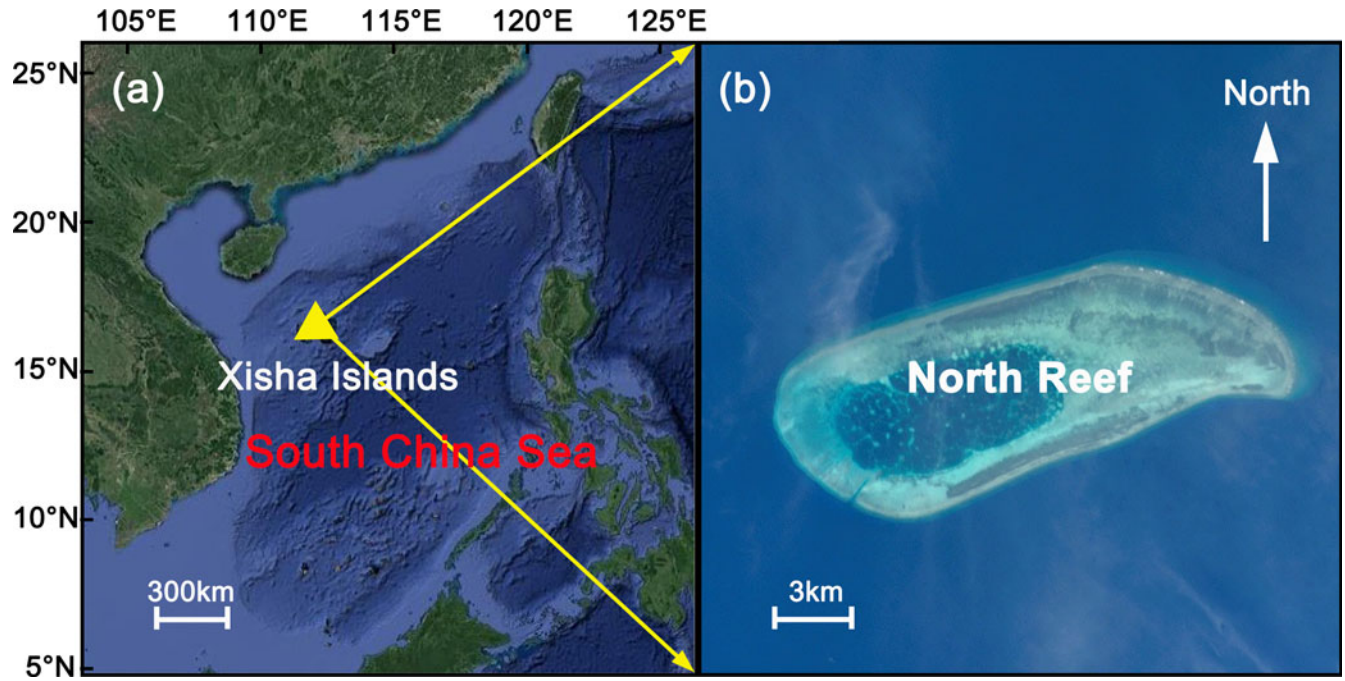

Figure 1. (a) Map of the South China Sea with location of the Xisha Islands marked by a yellow triangle. Yellow arrows represent that map b is an inset from map a. (b) Satellite photo of North Reef in the Xisha Islands.

https://doi.org/10.1017/qua.2021.28 Published online by Cambridge University Press

is connected with the Pacific Ocean to the east and the Indian Ocean to the west. The Xisha Islands (aka Paracel Islands; located ~111°E to ~113°E, ~15°40′N to ~17°10′N; Fig. 1a), are a SCS island group, and are located in the northwest SCS. North Reef (111°30′E, 17°05′N; Fig. 1b) is located in the northern part of Xisha Islands and is a tropical elliptic coral reef.

The climate of the Xisha Islands, which is strongly influenced by the Asian monsoon, has obvious seasonal climate changes. Figure 2 shows the mean SST distribution map in January and June from the SCS from AD 1955–2012 (Fig. 2a, b) and the average monthly time-series of air temperature (AT), SST, and precipitation from AD 2000–2016 (Fig. 2c, d). From AD 2000–2016 the lowest monthly SST in the Xisha Islands occurred in January (24.75°C) and the highest monthly SST occurred in June (29.51°C) (Fig. 2c). Due to the influence of the southwest Asian monsoon, rain in the Xisha Islands mainly falls from June to November, and rarely from December to May (Fig. 2d). Thus, the climate of Xisha Islands has distinct dry and wet seasons. The monthly SST and precipitation data in Xisha Islands used in this study were obtained from the Asia-Pacific Data-Research Center with a spatial resolution of 1°×1° (http://apdrc.soest.hawaii.edu/data/data.php?discipline_index=2, accessed October 15, 2020). For SST and precipitation data, we chose the HadlSST and CPC databases. The AT data in Xisha Islands was obtained from meteorological observations from the China greenhouse data-sharing platform (http://data.sheshiyuanyi.com/WeatherData/, accessed July 18, 2020).

Shell collection and sample preparation

For this study, four *Tridacna* spp. specimens were used in our analyses. One modern specimen (YX1; published in Yan et al., 2013), was collected alive from Yongxing Island, Xisha Islands, SCS, in March 2005. The other three subfossil *Tridacna squamosa* (specimens A87, A165 and A276; Fig. 3), were collected from North Reef, Xisha Islands, SCS, in April 2015. By cutting along the maximum growth axis, longitudinal sections of shells were obtained. Clear growth laminae were visible in the sections (Fig. 3).

Consistent with previous studies (Watanabe et al., 2004; Yan et al., 2013, 2014b, 2014c, 2015), X-ray diffraction analysis showed that the *Tridacna squamosa* shells studied herein were mainly aragonitic. To remove organic matter from the surface of the sample slices, the slices were soaked in 30% hydrogen peroxide, then cleaned with deionized water using ultrasonic agitation, then air-dried (Yu et al., 2005a; Goodkin et al., 2005).

AMS ^{14}C dating and Sr/Ca analysis

Accelerator-based mass spectroscopic (AMS) ^{14}C measurements and Sr/Ca analysis were completed at the Institute of Earth Environment, Chinese Academy of Sciences (IEECAS). Powder samples collected from the middle of the sections of the three subfossil *Tridacna squamosa* specimens (A87, A165, and A276) were used for AMS ^{14}C measurements. Each subsample required ~ 0.1 g for CO_2 generation. The powder samples were placed in a mass spec, then pumped down to achieve a vacuum and the 85% orthophosphoric acid added to generate CO_2 (Griffin and Druffel., 1985). The resulting CO_2 was purified through a vacuum line. We used a zinc reduction method to convert the CO_2 to graphite (Xu et al., 2007), then the graphite was analyzed by AMS ^{14}C measurements.

The powder samples used for Sr/Ca analysis were obtained along the maximum growth axis and perpendicular to the annual lamina using a micro mill to create powder along a groove (Yan et al., 2013, 2014b, 2015). Groove cross-section lengths were

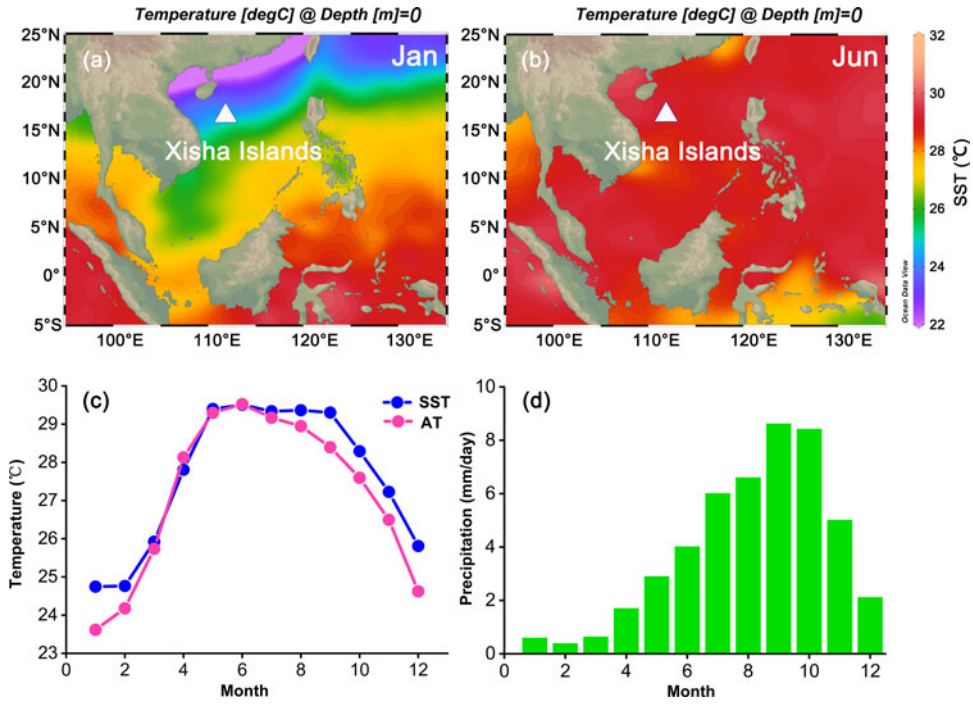

Figure 2. Mean sea-surface temperature (SST) distribution map of the South China Sea in (a) January [Jan] and (b) June [Jun] from AD 1955 to AD 2012. Location of Xisha Islands is marked by a white triangle. (c) Monthly mean air temperature (AT) and SST from AD 2000 to AD 2016, and (d) monthly mean precipitation from AD 2000 to AD 2016.

https://doi.org/10.1017/qua.2021.28 Published online by Cambridge University Press

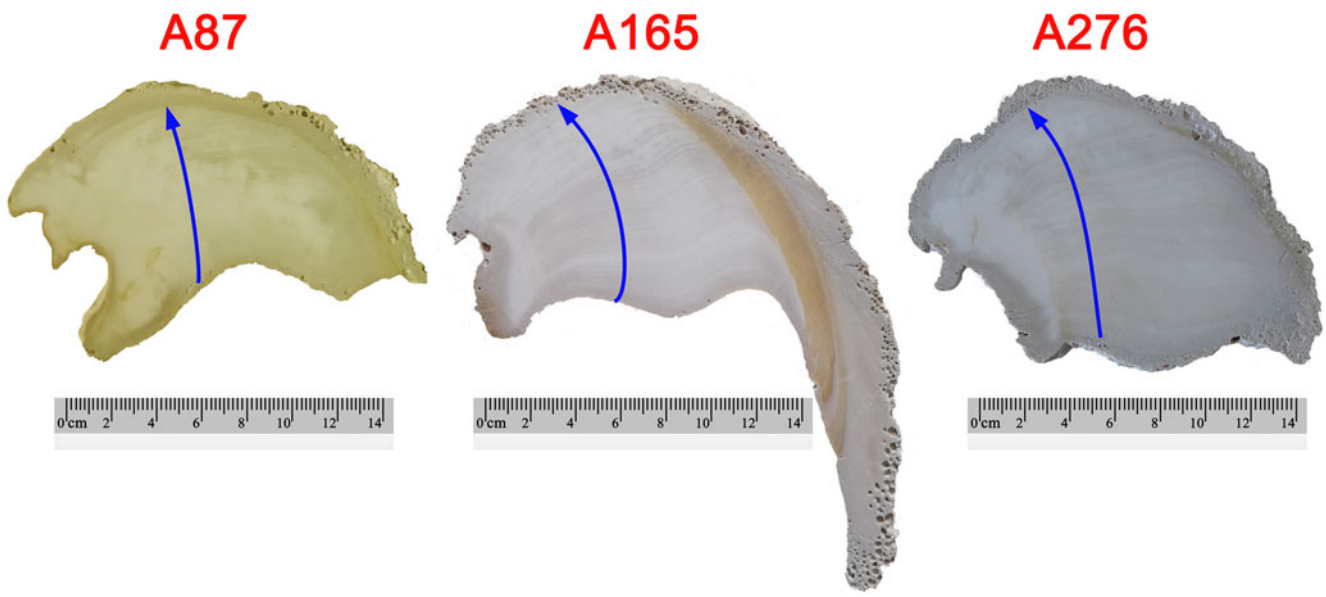

Figure 3. Longitudinal sections of *Tridacna squamosa* specimens A87, A165, and A276 used in this study. Blue lines indicate the track of the sampling lines used for Sr/Ca determination.

2 mm and widths were 0.15 mm, then 12–30 powder samples were obtained from each annual layer for Sr/Ca determination. A total of 2452 samples were obtained for Sr/Ca analysis: 622 for A87, 810 for A165, and 1020 for A276. Approximately 0.5–1.5 mg of each powder sample was dissolved in 2 ml 5% HNO_3, and 1.5 ml of this solution was then used for the Sr/Ca measurements. The Sr/Ca ratios were determined by ICP-OES with radial plasma observation (identified spectral lines for Ca: 317.933 nm, and for Sr: 407.711 nm). In order to ensure the stability of the measurements, we inserted a laboratory standard sample after every five subsamples to check accuracy of the measurements. The external precision of a laboratory standard was ± 0.79% for Sr/Ca.

Establishing chronologies of Sr/Ca profiles

Chronological frameworks for the Sr/Ca profiles of *Tridacna squamosa* specimens A87, A165, and A276 were established using the method described by Yan et al. (2013). A recent study by Arias-Ruiz et al. (2017) showed that the Sr/Ca profiles of *Tridacna squamosa* shells have a significant positive correlation with the local SST and that the lowest Sr/Ca ratios correspond to the coldest season of a year. Chronologies for high-resolution Sr/Ca profiles of *Tridacna squamosa* shells A87, A165, and A276 were established using annual arrival times of the winter SST minima in Xisha Islands (which was then assigned as January), then the time between the Sr/Ca minima was assigned using linear interpolation with an equal timespan (Sun et al., 2005; Yan et al., 2013).

Data resampling

Because the number of sampling intervals between each layer differed, in order to assess the past seasonal climate changes from the Sr/Ca ratios of *Tridacna squamosa* specimens, Sr/Ca data were resampled with a 12-point cubic spline model (Wanamaker et al., 2011), using AnalySeries (Paillard et al., 1996; http://www.lsce.ipsl.fr/en/softwares/index.php).

Calculating SST seasonality

Seasonality was generally defined as the difference between summer and winter values in any given year. The Sr/Ca profiles of the *Tridacna* specimens used in this study showed clear annual cycles, and we defined the Sr/Ca seasonality (ΔSr/Ca) as the difference between the average of three maximum Sr/Ca ratios (mean of June, July and August = summer) and the average of two minimum Sr/Ca ratios (mean of January and February = winter) for each year. Previous studies have demonstrated that seasonal variations of *Tridacna* Sr/Ca in the northern SCS were primarily controlled by seasonal oscillations of the SST, and Sr/Ca-SST slopes were similar among species and individuals of *Tridacna* shells (Yan et al., 2014a). Thus, the SST seasonality ΔT (°C) in the northern SCS can be calculated from the Sr/Ca seasonality (ΔSr/Ca) of *Tridacna* shells using the following equation by Yan et al. (2013):

$$\text{SST seasonality } \Delta T\ (^{\circ}\text{C}) = \text{proxy seasonality } \Delta\text{Sr/Ca} \times 16.60 \quad \text{(Eq. 1)}$$

RESULTS

AMS ^{14}C dating

Results from age-dating the studied *Tridacna* specimens are shown in Table 1. The modern *Tridacna gigas* specimen YX1, collected live in March 2005, had a growth period from AD 1994–2005. The AMS ^{14}C dating results of three sub-fossil *Tridacna squamosa* specimens were: A87, 3304 ± 80 ^{14}C yr BP; A165, 4063 ± 60 ^{14}C yr BP; and A276, 4653 ± 60 ^{14}C yr BP. The AMS ^{14}C ages were calibrated by the marine ^{14}C yield model using Marine13 of Calib Rev. 7.0.4 (http://www.calib.org, accessed August 12, 2020) with a regional ΔR = 18 and σ = 37 (Southon et al., 2002), resulting in calibrated ages of: A87, 3118 ± 80 cal yr BP; A165, 4069 ± 60 cal yr BP; and A276, 4860 ± 60 cal yr BP.

Sr/Ca ratios for specimens A87, A165 and A276

The Sr/Ca ratios for specimens A87, A165, and A276 were: 1.23–1.81 mmol/mol, 1.39–2.00 mmol/mol and 1.26–1.75 mmol/mol;

https://doi.org/10.1017/qua.2021.28 Published online by Cambridge University Press

Table 1. Results from AMS ^{14}C dating and Sr/Ca ratios.

Sample ID	^{14}C Age	Cal ^{14}C Age	Error (2σ)	Record length (yr)	Mean Sr/Ca (mmol/mol)	Sr/Ca STD (1σ)	Sampling resolution (samples/yr)
YX1	1994–2005 AD	1994–2005 AD	0	11	2.234	0.102	17.4
A87	3304 yr BP	3118 yr BP	80	34	1.520	0.098	18.3
A165	4063 yr BP	4069 yr BP	60	36	1.663	0.107	22.5
A276	4653 yr BP	4860 yr BP	60	53	1.475	0.091	19.2

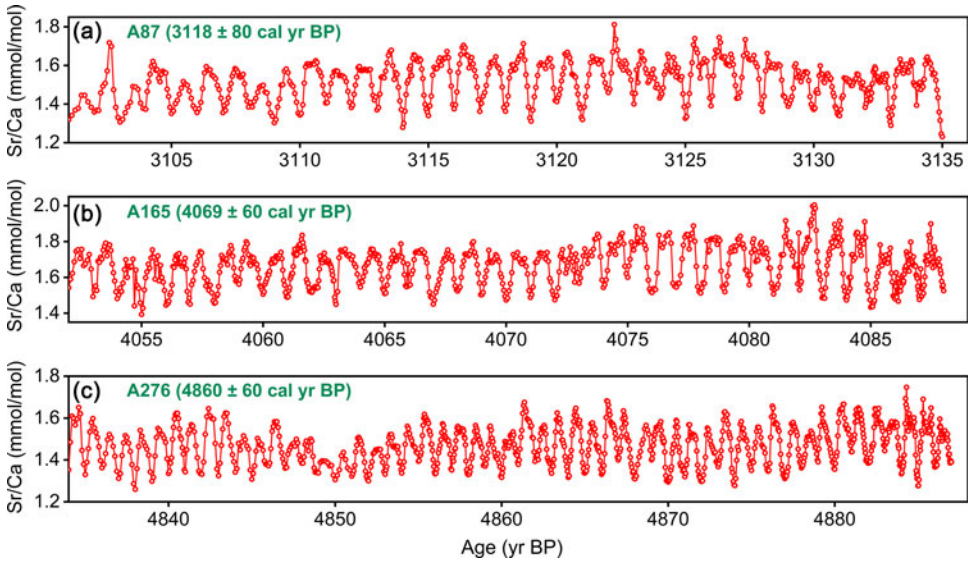

Figure 4. Sr/Ca profiles plotted against calibrated ages of *Tridacna squamosa* specimens: (a) A87, (b) A165, and (c) A276.

the means were 1.52 ± 0.10 mmol/mol (n = 622), 1.66 ± 0.11 mmol/mol (n = 810) and 1.48 ± 0.09 mmol/mol (n = 1020), respectively (Fig. 4, Table. 1). 34, 36, and 53 annual cycles were identified from the Sr/Ca profiles of A87, A165, and A276, respectively.

Data resampling and calculated proxy SST seasonality

For the three subfossil *Tridacna squamosa* specimens, 12 to 42 Sr/Ca samples were obtained from each annual layer. To assess changes in the seasonal SST cycle, the number of Sr/Ca samples per year was adjusted to 12 points using a 12-point cubic spline model resampling (Wanamaker et al., 2011). The results of 12-point resampling for Sr/Ca profiles of *Tridacna squamosa* specimens A87, A165, and A276 are shown in Figure 5.

The ΔSr/Ca and calculated SST seasonality of *Tridacna squamosa* specimens A87, A165, and A276 are plotted in Figure 6. The mean SST seasonality of specimens A87, A165, and A276 were 3.13 ± 1.00°C (mean ΔSr/Ca = 0.19 ± 0.06 mmol/mol), 3.59 ± 0.98°C (mean ΔSr/Ca = 0.22 ± 0.06 mmol/mol), 3.00 ± 0.89°C (mean ΔSr/Ca = 0.18 ± 0.05 mmol/mol), respectively.

In order to test the SST seasonality differences between the middle Holocene and present, the SST seasonality from AD 1994–2004 was calculated using the published Sr/Ca data from a modern *Tridacna gigas* specimen (YX1, Yan et al., 2013) and instrumental data. The averaged SST seasonality from AD 1994–2004 derived from YX1 and instrumental data were 4.05 ± 0.69°C and 4.32 ± 0.59°C, respectively. The averaged SST seasonality during the middle Holocene derived from the three *Tridacna squamosa* specimens in this study was 3.21 ± 0.98°C, indicating a smaller SST seasonality during the middle Holocene than that during AD 1994–2004 (Fig. 7).

DISCUSSION

Reconstructing SST seasonality using Sr/Ca ratios from Tridacna *shells*

The Sr/Ca ratios of coral skeletons have long been known to yield a high-resolution proxy for SST, and thus have been extensively utilized in high-resolution paleotemperature reconstructions in tropical oceans (Beck et al., 1992; McCulloch et al., 1994; de Villiers et al., 1995; McCulloch et al., 1996; Alibert and McCulloch, 1997; de Villiers, 1999). Coral Sr/Ca ratios in the northern SCS have been widely studied, and the calibration between modern coral and instrumental data shows that the coral Sr/Ca ratio in the northern SCS is highly correlated with local SST and can be used as a monthly resolution SST proxy (Wei et al., 2000, 2004; Yu et al., 2005a; Chen et al., 2013). An early study suggested that the monthly resolution Sr/Ca profile of *Tridacna squamosa* from the SCS showed clear annual cycles and had a significant correlation with the local instrumental SST record, indicating that the Sr/Ca ratio from *Tridacna squamosa* had potential to become an indicator of SST variations (Shao et al., 2012). Subsequent studies have shown that the Sr/Ca ratios of *Tridacna gigas* and *Tridacna derasa* also indicated clear annual cycles and were significantly correlated with the local SST (Yan et al., 2014a, 2015). Several recent

https://doi.org/10.1017/qua.2021.28 Published online by Cambridge University Press

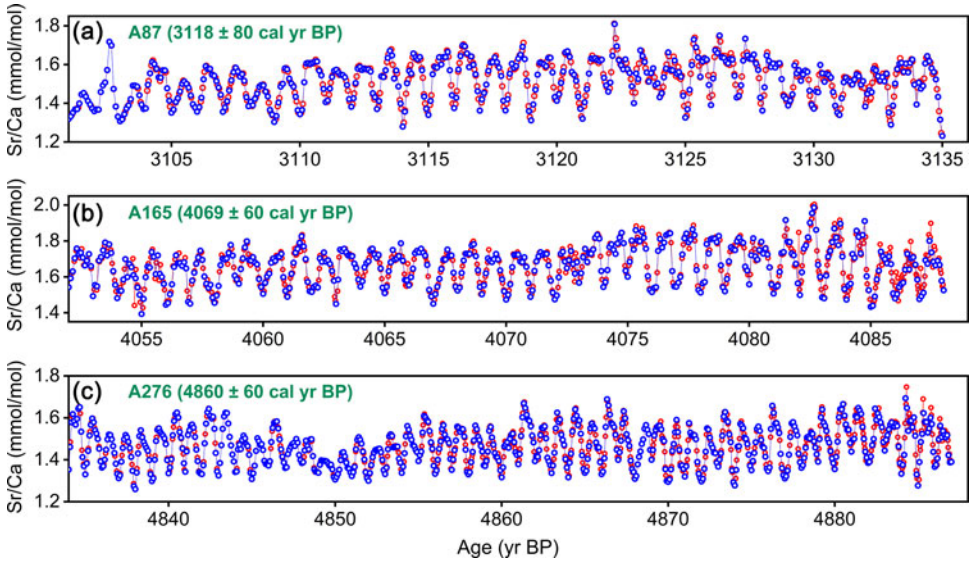

Figure 5. Profiles from the 12-point resampling for Sr/Ca profiles plotted against calibrated ages of *Tridacna* specimens (a) A87, (b) A165, and (c) A276. Original Sr/Ca data are shown in red and resamples data are in blue.

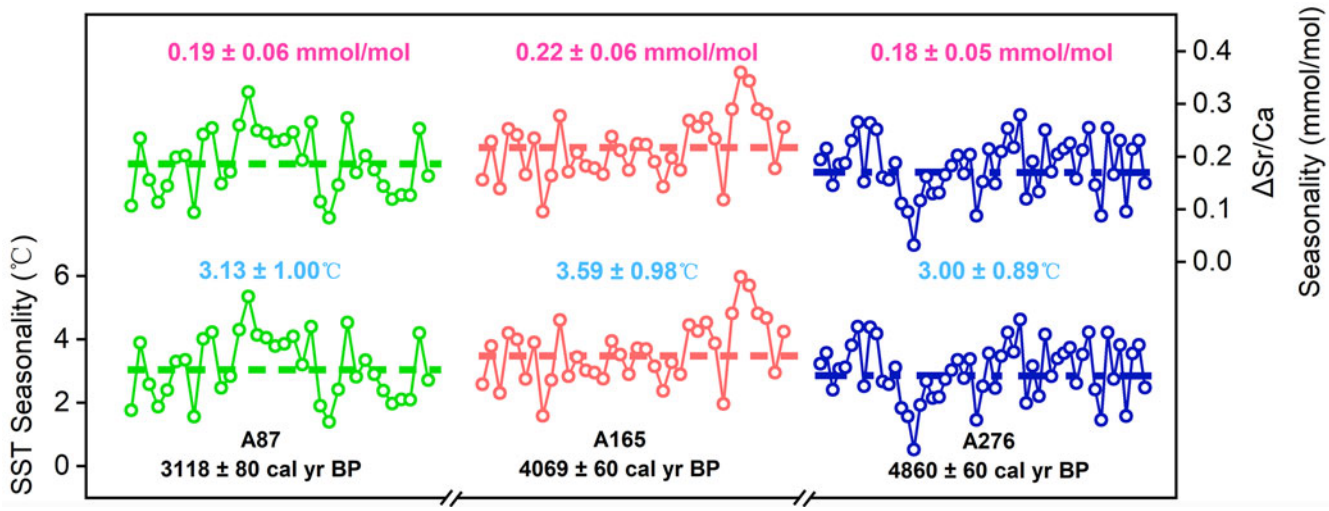

Figure 6. Seasonality reconstruction inferred using ΔSr/Ca from *Tridacna squamosa* specimens A87, A165, and A276. SST = sea surface temperature.

studies showed that the high-resolution Sr/Ca ratios of *Tridacna* shells in the northern SCS also can capture a full annual cycle (Yan et al., 2013, 2014a, 2015). Although substantial differences of mean Sr/Ca values were observed among *Tridacna* species in the northern SCS, Yan et al. (2014a) found that the slopes of SST to Sr/Ca among *Tridacna* species were relatively similar, indicating that the Sr/Ca in *Tridacna* shells can be used to reconstruct SST seasonality in the northern SCS, and is not affected by species (Yan et al., 2014a).

In order to test the reliability of SST seasonality reconstruction from *Tridacna* shells, the Sr/Ca data of a modern *Tridacna gigas* specimen (YX1, Yan et al., 2013) were repeated in this study. Figure 8a shows the significant correlation between high-resolution Sr/Ca data of YX1 and modern instrumental SST data at Xisha Islands from AD 1994–2004 ($R = -0.83$, $P < 0.001$, $n = 121$). Based on Equation 1, the mean proxy-SST seasonality calculated from ΔSr/Ca of YX1 was 4.05 ± 0.69°C, which showed a significant correlation ($R = 0.64$, $P < 0.05$, $n = 11$) with modern instrumental SST seasonality (4.32 ± 0.59°C) from AD 1994–2004 from the Xisha Islands (Fig. 8b, c). This finding also supports that the *Tridacna* shell Sr/Ca has the potential to be used as an SST seasonality proxy.

Recent decadal variations and dynamics of SST seasonality in the northern SCS

In order to understand changes of SST seasonality in the middle Holocene, the variations and dynamics of high-resolution instrumental SST seasonality in the northern SCS were investigated. The relationship between the SST seasonality and the SST in summer, winter, and annually were also calculated to test the contribution of summer, winter, and annual SST to changes in SST seasonality. The results revealed a negative correlation between SST seasonality and annual SST ($R = -0.44$, $P < 0.05$; Fig. 9a),

https://doi.org/10.1017/qua.2021.28 Published online by Cambridge University Press

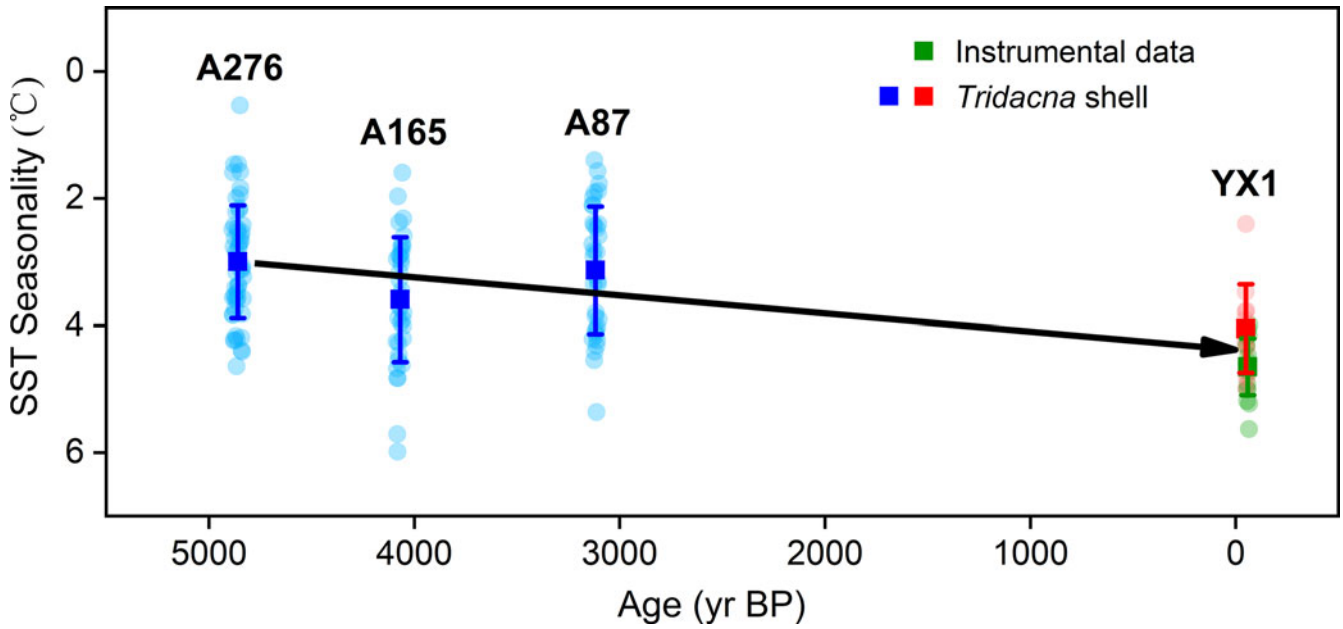

Figure 7. Sequence of sea surface temperature (SST) seasonality reconstructions for the three *Tridacna squamosa* samples used in this study (A276, A165, A87), *Tridacna gigas* YX1 (Yan et al., 2013), and modern instrumental data. The mean SST seasonality of the three *Tridacna squamosa* in this study, the *Tridacna gigas* YX1, and modern instrumental data from Xisha Islands of the north SCS are marked by blue, red and green squares, respectively. Error bar (1σ) is the standard deviation of the SST seasonality.

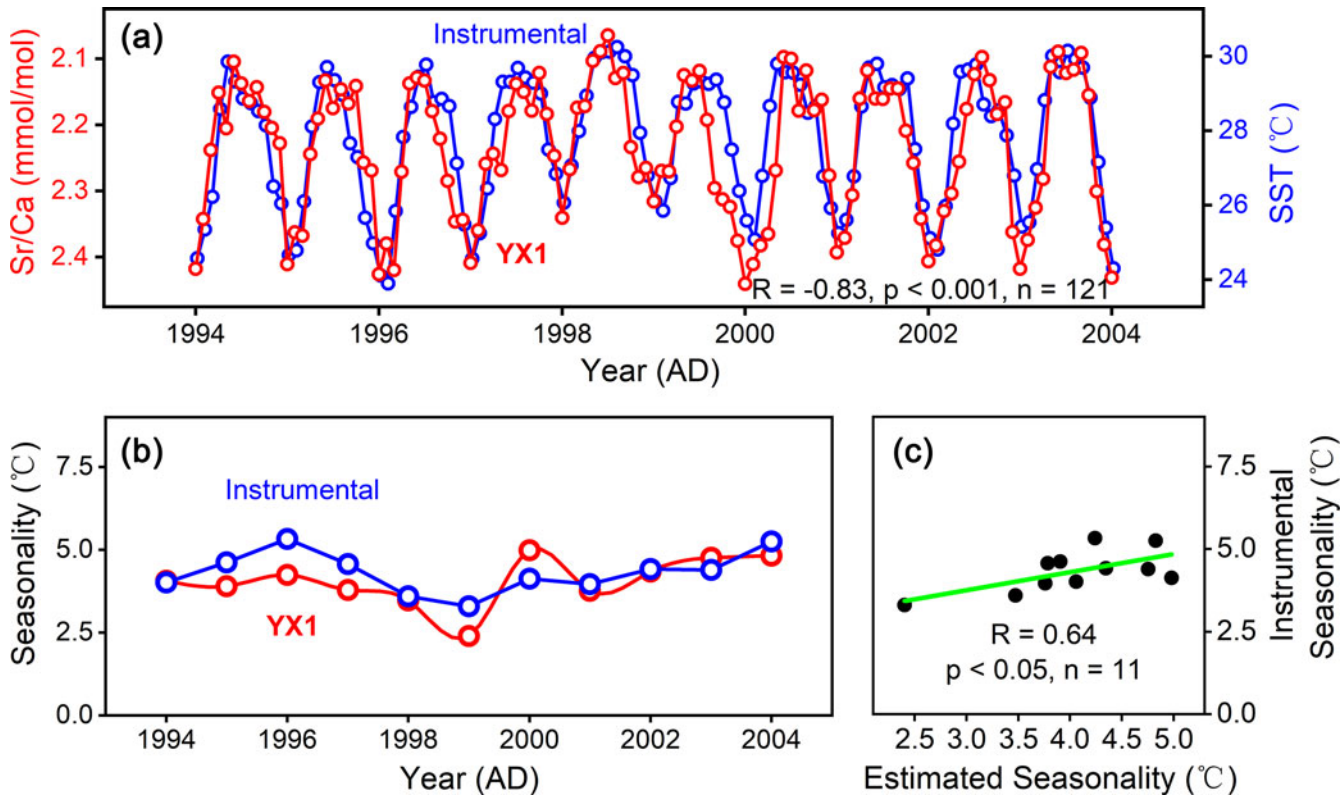

Figure 8. (a) Instrumental sea surface temperature (SST; blue) and Sr/Ca data from sample YX1 (red) during AD 1994–2004. (b) Instrumental seasonality (blue) and estimated seasonality (red) based on Sr/Ca data from sample YX1 during AD 1994–2004. (c) Linear regression (green solid line) between the estimated seasonality and the instrumental seasonality. This figure is reproduced from Yan et al., 2015.

https://doi.org/10.1017/qua.2021.28 Published online by Cambridge University Press

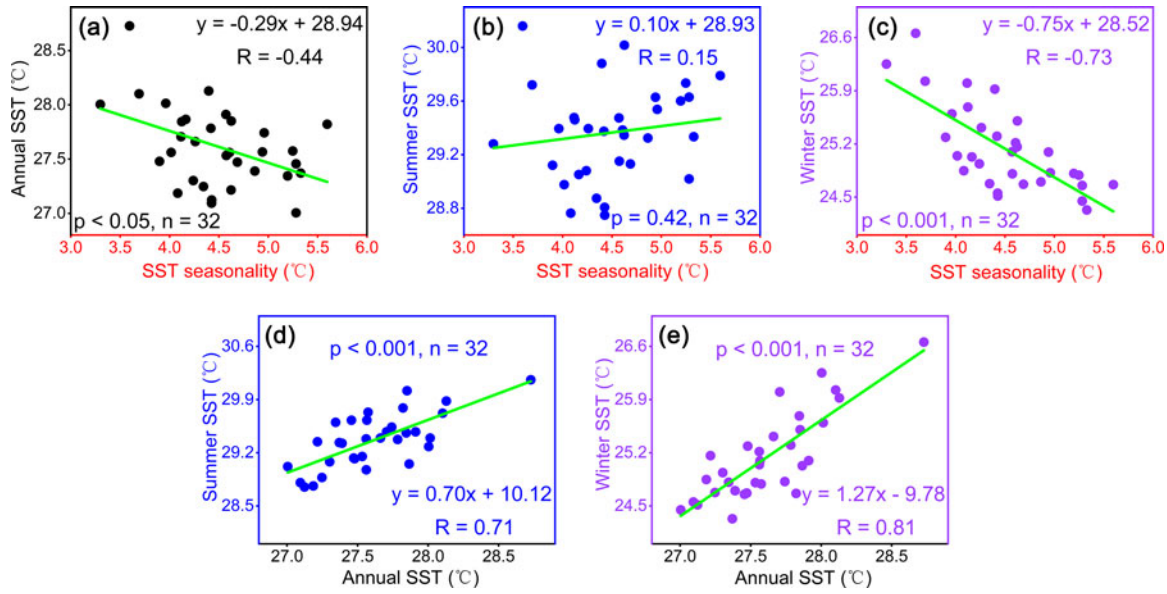

Figure 9. Estimated high-resolution instrumental sea surface temperature (SST) data AD 1983–2014. Relationship between instrumental SST seasonality and: (a) annual SST, (b) summer SST, and (c) winter SST from the Xisha Islands, northern South China Sea (SCS). Relationship between instrumental annual SST and: (d) summer SST, and (e) winter SST in the Xisha Islands, northern SCS. Correlation lines shown in green. Modern instrumental SST data from the Xisha Islands was obtained from meteorological observations of the China greenhouse data sharing platform (http://data.sheshiyuanyi.com/WeatherData/).

which indicated that the SST seasonality decreased in response to warmer mean climate conditions. The SST seasonality showed no significant correlation with summer SST ($R = 0.15$, $P = 0.42$; Fig. 9b), but was highly correlated with winter SST ($R = -0.73$, $P < 0.001$; Fig. 9c), indicating that the SST seasonality in the northern SCS probably depended on the variability of winter conditions. The instrumental SST data also suggested that the annual SST increase/decrease of 1°C could result from winter SST and summer SST increase/decrease of 1.27°C and 0.70°C, respectively (Fig. 9d, e). Therefore, the asynchronicity between SST in winter and summer could explain the negative correlation between SST seasonality and annual mean SST in the northern SCS. When the climate in the northern SCS warmed, the rising range of SST during summer was less than that during winter, resulting in a reduction of the amplitude of SST seasonality.

SST in summer and winter was probably influenced by different climate dynamics in the northern SCS. During the summer, the western Pacific warm pool (WPWP) expanded northward to include the SCS, so summer SST in the northern SCS was likely controlled by this shift. During the winter, the WPWP center shifted south towards the equator, and the SCS was 'engulfed' by mid-high latitude southward-moving cold water driven by the East Asian winter monsoon (EAWM). Thus, the intensity of EAWM probably had a significant influence on winter SST, which would further affect the SST seasonality in the northern SCS. This scenario was also evident in the instrumental records from AD 1961 to AD 1999 (Fig. 10), which suggested that winter SST in the northern SCS was negatively correlated with the EAWM strength ($R = -0.58$, $P < 0.001$, $n = 38$). The winter monsoon velocity (WMV; December-January-February) from Yongxing Island was used as a proxy of the EAWM strength of the northern SCS (Fig. 10).

In short, high-resolution modern instrumental data suggest that the SST seasonality in the northern SCS was negatively correlated with annual SST in the SCS. When annual SST increased,

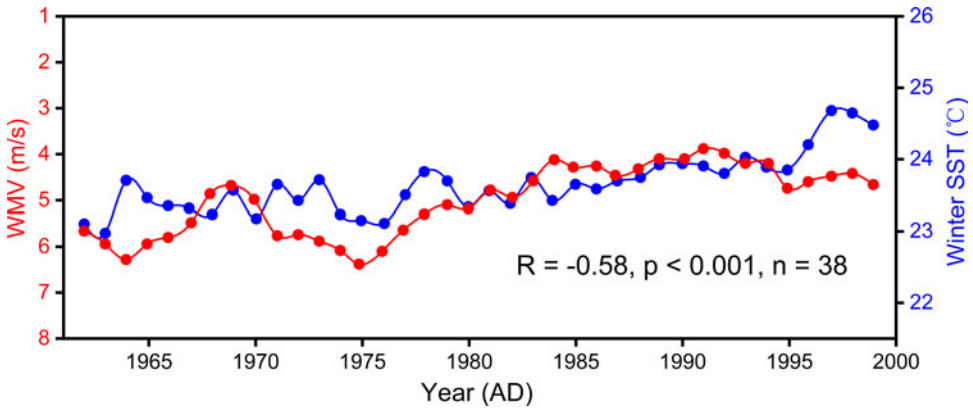

Figure 10. Relationship between winter monsoon velocity (WMV; red) and instrumental winter sea surface temperature (SST; blue) from AD 1961–1999. WMV data (December–February) were obtained from an observation station in the Xisha Islands available at http://data.cma.cn/data.

https://doi.org/10.1017/qua.2021.28 Published online by Cambridge University Press

SST seasonality generally decreased, and vice versa. The negative correlation between annual SST and SST seasonality was mainly caused by asynchronicity of SST variations in winter and summer. When the northern SCS mean climate condition warmed, winter SST increased more than that in summer, resulting in a reduction of the amplitude of SST seasonality. When the northern SCS mean climate conditions cooled, the decreased amplitude of SST in winter was larger than that in summer, resulting in an increased SST seasonality. Therefore, the SST seasonality in the northern SCS was probably driven by winter SST. The variation of winter SST in the northern SCS was deeply influenced by the intensity of EAWM.

Reconstructed SST seasonality in the northern SCS during the middle Holocene

Based on the high-resolution monthly Sr/Ca from three middle Holocene *Tridacna squamosa* specimens (A87, A165, and A276) from North Reef, northern SCS, the SST seasonality of three time-windows from the middle Holocene was reconstructed.

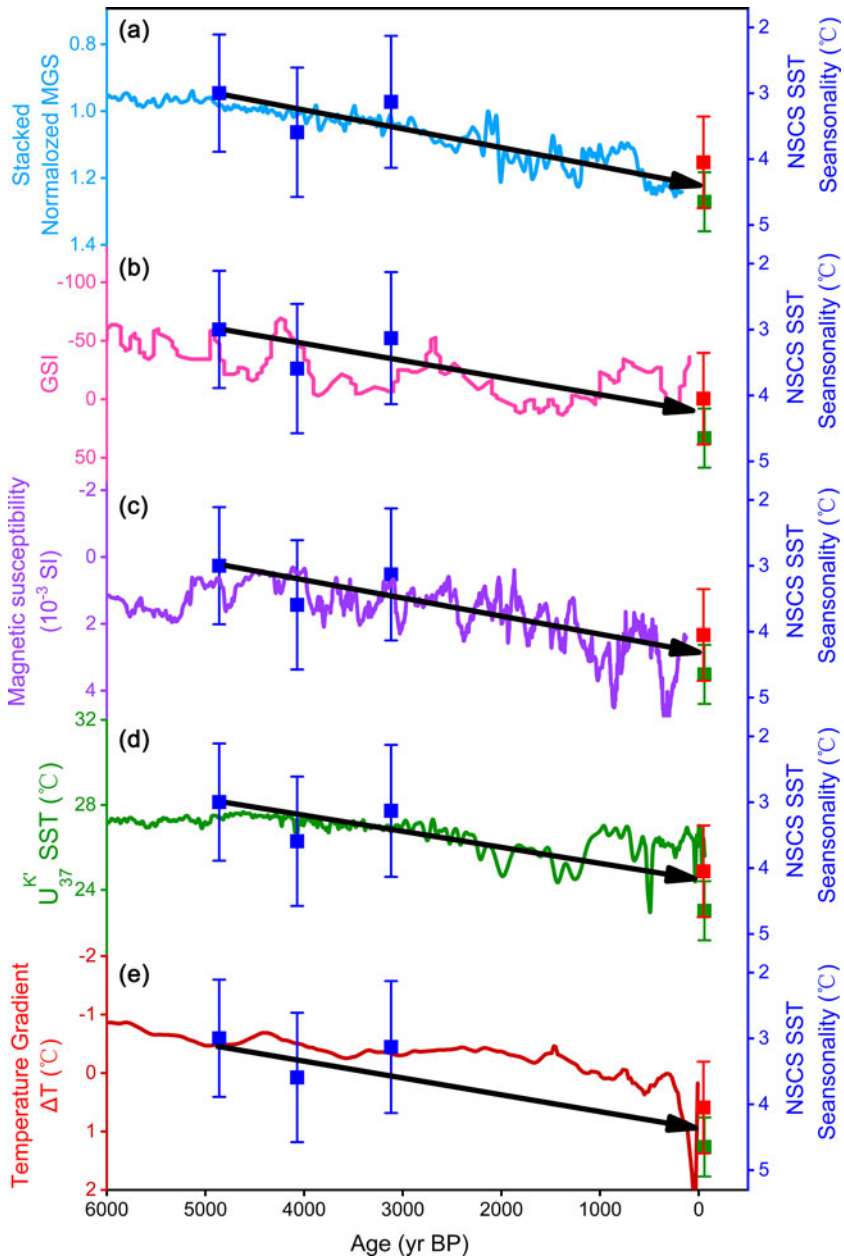

Figure 11. Comparing sea surface temperature (SST) seasonality records (squares) in the northern South China Sea (NSCS) during the middle to late Holocene with other published paleoclimate records. Holocene East Asian winter monsoon (EAWM) records derived from (a) mean grain size (MGS) of Chinese loess sediment (Kang et al., 2020), (b) grain-size index (GSI) from core Oki02 in the northwestern Pacific Ocean (Zheng et al., 2014), and (c) magnetic susceptibility of a sediment core from Lake Huguang Maar (Yancheva et al., 2007). (d) Reconstruction of Holocene mean annual SST in the northern SCS derived from long-chain unsaturated alkenones $U^{K'}_{37}$ (Zhang et al., 2019). (e) Temperature gradient between the low and high latitudes of Northern Hemisphere (Marcott et al., 2013). Blue squares indicate the average SST seasonality derived from the Sr/Ca ratio of middle Holocene *Tridacna squamosa* specimens (A87, A165, and A276), red squares indicate the Sr/Ca ratio of a modern *Tridacna gigas* specimen (YX1), and green squares indicate modern instrumental SST data (AD 1994–2004).

https://doi.org/10.1017/qua.2021.28 Published online by Cambridge University Press

The results indicated that the SST seasonality in the northern SCS during the middle Holocene (3.21 ± 0.98°C) was smaller than that for recent decades (AD 1994–2004, 4.32 ± 0.59°C).

Instrumental data suggested that the SST seasonality in the northern SCS was dominated by the winter SST, which was deeply influenced by the EAWM. Thus, the small SST seasonality changes in the northern SCS during the middle Holocene probably indicated a warmer winter SST and a weaker EAWM in the northern SCS during the middle Holocene than that during AD 1994–2004. However, this hypothesis was difficult to test due to the limitation of the high-resolution seasonal SST records from the northern SCS. In contrast to the lack of the seasonal temperature records, the evolution of the EAWM during the Holocene has been widely investigated. Thus, we compared our Holocene SST seasonality data with the EAWM reconstructions derived from the mean grain size of Chinese loess sediment (Kang et al., 2020; Fig. 11a), grain-size index from core Oki02 in northwestern Pacific Ocean (Zheng et al., 2014; Fig. 11b) and the magnetic susceptibility of a sediment core from Lake Huguang Maar (Yancheva et al., 2007; Fig. 11c). All of these paleoclimate records showed that the EAWM strengthened from the middle Holocene to the present, which probably led to a decrease of the winter SST in the northern SCS and resulted in a larger SST seasonality. This may be the reason for the smaller SST seasonality changes during the middle Holocene recorded in our *Tridacna* specimen records. A recent reconstruction of the Holocene mean annual SST in the northern SCS derived from the long-chain unsaturated alkenones $U^{K'}_{37}$ emphasized the more important role of winter temperatures, and indicated a warmer SST during the middle Holocene (Zhang et al., 2019; Fig. 11d), also consistent with our deductions. We also calculated the temperature difference between the low and mid-high latitudes of the Northern Hemisphere (ΔT (°C) = $T_{30°S-30°N} - T_{90°N-30°N}$) (Marcott et al., 2013) and found that the temperature gradient increased from the middle Holocene to present, also supporting an increased EAWM and enhanced SST seasonality in the northern SCS from the middle to late Holocene (Fig. 11e). The increased EAWM from the middle to late Holocene was probably associated with the continued increased temperature gradient between low and mid-high latitudes of the Northern Hemisphere. Compared with the slight temperature changes in low latitudes, the temperature gradient between low and mid-high latitudes in the Northern Hemisphere was primarily determined by mid-high latitudes in the Holocene (Marcott et al., 2013). Therefore, decreases of temperature in mid-high latitudes of the Northern Hemisphere could strengthen the Siberian High, which in turn could increase the temperature gradient between the low and mid-high latitudes (Kang et al., 2020). In addition, because of the thermodynamic difference between land and sea, the gradient between the Aleutian Low and Siberian High accordingly changed, an important reason for increased intensity of the EAWM. In contrast, the increase in the temperatures of mid-high latitudes of the Northern Hemisphere weakened the EAWM. Therefore, the continued increased temperature gradient between the low and mid-high latitudes of the Northern Hemisphere during the middle to late Holocene may be the reason for the increase in EAWM intensity (Fig. 11e).

It is worth noting that only three *Tridacna* high resolution time-windows with a total of 123 years were determined in our study, which limited a comprehensive understanding of the regional climate changes during the middle to late Holocene. In addition, it is almost impossible to produce continuous monthly resolution *Tridacna* records during the Holocene due to the relatively short lifespan of *Tridacna* (most live < 100 years), dating errors, and the huge workload of determinations. However, our study demonstrated that the combination of high- and low-resolution paleoclimate records can provide more details for past climate changes and greatly improve our understanding of the climate dynamics.

CONCLUSION

High-precision monthly resolution Sr/Ca ratios of three *Tridacna squamosa* specimens (A87, A165, A276) were determined to estimate SST seasonality during the middle Holocene. The results suggested that SST seasonality in the northern SCS during the middle Holocene was less pronounced than that during AD 1994–2004. We inferred that the less-pronounced SST seasonality during the middle Holocene was probably induced by higher winter SST, which was linked with a weaker EAWM and smaller high- to low-latitude temperature gradient in the Northern Hemisphere. Our study highlights that high-resolution *Tridacna* Sr/Ca records, together with other low-resolution paleoclimate records, can provide more evidence to help understand the variations and dynamics of past climate changes in the northern SCS.

Supplementary Material. The supplementary material for this article can be found at https://doi.org/10.1017/qua.2021.28.

Financial Support. Financial support for this research was provided by the National Natural Science Foundation of China (NSFC) (41877399, 42025304, 41991250), the Research Projects from Chinese Academy of Sciences (XDB40000000), the "Light of West China" Program of the Chinese Academy of Sciences, and the National Key R&D Program of China (2019YFC1509100).

REFERENCES

Aharon, P., 1983. 140,000-yr isotope climatic record from raised coral reefs in New Guinea. *Nature* **304**, 720–723.

Aharon, P., 1991. Recorders of reef environment histories: stable isotopes in corals, giant clams, and calcareous algae. *Coral Reefs* **10**, 71–90.

Aharon, P., Chappell, J., 1986. Oxygen isotopes, sea level changes and the temperature history of a coral reef environment in New Guinea over the last 10^5 years. *Palaeogeography, Palaeoclimatology, Palaeoecology* **56**, 337–379.

Alibert, C., McCulloch, M.T., 1997. Strontium/calcium ratios in modern *Porites* corals from the Great Barrier Reef as a proxy for sea surface temperature: Calibration of the thermometer and monitoring of ENSO. *Paleoceanography and Paleoclimatology* **12**, 345–363.

Andreasson, F.P., Schmitz, B., 2000. Temperature seasonality in the early middle Eocene North Atlantic region: Evidence from stable isotope profiles of marine gastropod shells. *Geological Society of America Bulletin* **112**, 628–640.

An, Z., Kukla, G., Porter, S., Xiao, J., 1991. Magnetic susceptibility evidence of monsoon variation on the Loess Plateau of central China during the last 130,000 years. *Quaternary Research* **36**, 29–36.

Arias-Ruiz, C., Elliot, M., Bézos, A., Pedoja, K., Husson, L., Cahyarini, S.Y., Cariou, E., Michel, E., La, C., Manssouri, F., 2017. Geochemical fingerprints of climate variation and the extreme La Niña 2010–11 as recorded in a *Tridacna squamosa* shell from Sulawesi, Indonesia. *Palaeogeography, Palaeoclimatology, Palaeoecology* **487**, 216–228.

Arthur, M.A., Williams, D.F., Jones, D.S., 1983. Seasonal temperature-salinity changes and thermocline development in the mid-Atlantic Bight as recorded by the isotopic composition of bivalves. *Geology* **11**, 655–659.

Ayling, B.F., Chappell, J., Gagan, M.K., McCulloch, M.T., 2015. ENSO variability during MIS 11 (424–374 ka) from *Tridacna gigas* at Huon Peninsula, Papua New Guinea. *Earth and Planetary Science Letters* **431**, 236–246.

Batenburg, S.J., Reichart, G., Jilbert, T., Janse, M., Wesselingh, F.P., Renema, W., 2011. Interannual climate variability in the Miocene: High

resolution trace element and stable isotope ratios in giant clams. *Palaeogeography, Palaeoclimatology, Palaeoecology* **306**, 75–81.

Beck, J.W., Edwards, R.L., Ito, E., Taylor, F.W., Recy, J., Rougerie, F., Joannot, P., Henin, C., 1992. Sea-surface temperature from coral skeletal strontium/calcium ratios. *Science* **257**, 644–647.

Bolton, A., Goodkin, N.F., Hughen, K., Ostermann, D.R., Vo, S.T., Phan, H.K., 2014. Paired *Porites* coral Sr/Ca and $\delta^{18}O$ from the western South China Sea: Proxy calibration of sea surface temperature and precipitation. *Palaeogeography, Palaeoclimatology, Palaeoecology* **410**, 233–243.

Brocas, W.M., Felis, T., Gierz, P., Lohmann, G., Werner, M., Obert, J.C., Scholz, D., Kölling, M., Scheffers, S.R., 2018. Last interglacial hydroclimate seasonality reconstructed from tropical Atlantic corals. *Paleoceanography and Paleoclimatology* **33**, 198–213.

Butler, P.G., Wanamaker, A.D., Scourse, J.D., Richardson, C.A., Reynolds, D.J., 2011. Long-term stability of $\delta^{13}C$ with respect to biological age in the aragonite shell of mature specimens of the bivalve mollusk *Arctica islandica*. *Palaeogeography, Palaeoclimatology, Palaeoecology* **302**, 21–30.

Chen, C.Y., McGee, D., Woods, A., Pérez, L., Hatfield, R.G., Edwards, R.L., Cheng, H., *et al.*, 2020. U-Th dating of lake sediments: Lessons from the 700 ka sediment record of Lake Junín, Peru. *Quaternary Science Reviews* **244**, 106422. https://doi.org/10.1016/j.quascirev.2020.106422.

Chen, F., Wu, W., Holmes, J.A., Madsen, D.B., Zhu, Y., Jin, M., Oviatt, C.G., 2003. A mid-Holocene drought interval as evidenced by lake desiccation in the Alashan Plateau, Inner Mongolia, China. *Chinese Science Bulletin* **48**, 1401. https://doi.org/10.1360/03wd0245.

Cheng, H., Edwards, R.L., Southon, J., Matsumoto, K., Feinberg, J.M., Sinha, A., Zhou, W., *et al.*, 2018. Atmospheric $^{14}C/^{12}C$ changes during the last glacial period from Hulu Cave. *Science* **362**, 1293–1297.

Chen, T.R., Yu, K., Chen, T., 2013. Sr/Ca–sea surface temperature calibration in the coral *Porites lutea* from subtropical northern South China Sea. *Palaeogeography, Palaeoclimatology, Palaeoecology* **392**, 98–104.

Dansgaard, W., Johnsen, S.J., Clausen, H.B., Dahl-Jensen, D., Gundestrup, N.S., Hammer, C.U., Hvidberg, C.S., *et al.*, 1993. Evidence for general instability of past climate from a 250-kyr ice-core record. *Nature* **364**, 218–220.

Deng, W., Wei, G., Zhao, J., Zeng, T., 2019. Anthropogenic effects on tropical oceanic climate change and variability: An insight from the South China Sea over the past 2000 years. *Quaternary Science Reviews* **206**, 56–64.

de Villiers, S., 1999. Seawater strontium and Sr/Ca variability in the Atlantic and Pacific oceans. *Earth and Planetary Science Letters* **171**, 623–634.

de Villiers, S., Nelson, B.K., Chivas, A.R., 1995. Biological controls on coral Sr/Ca and $\delta^{18}O$ reconstructions of sea surface temperatures. *Science* **269**, 1247–1249.

Driscoll, R., Elliot, M., Russon, T., Welsh, K., Yokoyama, Y., Tudhope, A., 2014. ENSO reconstructions over the past 60 ka using giant clams (*Tridacna* spp.) from Papua New Guinea. *Geophysical Research Letters* **41**, 6819–6825.

Eawag, A.F.L., Eicher, U., Siegenthaler, U., Birks, H.J.B., 1992. Late-glacial climatic oscillations as recorded in Swiss lake sediments. *Journal of Quaternary Science* **7**, 187–204.

Elliot, M., Welsh, K., Chilcott, C., McCulloch, M., Chappell, J., Ayling, B., 2009. Profiles of trace elements and stable isotopes derived from giant long-lived *Tridacna gigas* bivalves: Potential applications in paleoclimate studies. *Palaeogeography, Palaeoclimatology, Palaeoecology* **280**, 132–142.

Fritts, H.C., Lofgren, G.R., Gordon, G.A., 1979. Variations in climate since 1602 as reconstructed from tree rings. *Quaternary Research* **12**, 18–46.

García-Escárzaga, A.G., Clarke, L.J., Gutiérrez-Zugasti, I., González-Morales, M., López-Higuera, J.M., Cobo, A., 2018. Mg/Ca profiles within archaeological mollusc (*Patella vulgata*) shells: Laser-induced breakdown spectroscopy compared to inductively coupled plasma-optical emission spectrometry. *Spectrochimica Part B: Atomic Spectroscopy* **148**, 8–15.

Goodkin, N.F., Hughen, K.A., Cohen, A.L., Smith, S.R., 2005. Record of Little Ice Age sea surface temperatures at Bermuda using a growth-dependent calibration of coral Sr/Ca. *Paleoceanography and Paleoclimatology* **20**, PA4016. https://doi.org/10.1029/2005PA001140.

Gorman, M.K., Quinn, T.M., Taylor, F.W., Partin, J.W., Cabioch, G., Austin, J.A., Pelletier, B., Ballu, V., Maes, C., Saustrup, S., 2012. A coral-based reconstruction of sea surface salinity at Sabine Bank, Vanuatu from 1842 to 2007 CE. *Paleoceanography and Paleoclimatology* **27**, PA3226. https://doi.org/10.1029/2012PA002302.

Griffin, S., and Druffel, E. 1985. Woods Hole Oceanographic Institution Radiocarbon Laboratory: sample treatment and gas preparation. *Radiocarbon* **27**, p. 43–51.

Hu, Y., Sun, X., Cheng, H., Yan, H., 2020. Evidence from giant-clam $\delta^{18}O$ of intense El Ninõ–Southern Oscillation-related variability but reduced frequency 3700 years ago. *Climate of the Past* **16**, 597–610.

Kang, S., Du, J., Wang, N., Dong, J., Wang, D., Wang, X., Qiang, X., Song, Y., 2020. Early Holocene weakening and mid- to late Holocene strengthening of the East Asian winter monsoon. *Geology* **48**, 1043–1047.

Kim, J., An, S., Jun, S., Park, H., Yeh, S., 2017. ENSO and East Asian winter monsoon relationship modulation associated with the anomalous northwest Pacific anticyclone. *Climate Dynamics* **49**, 1157–1179.

Liu, C., Yan, H., Fei, H., Ma, X., Zhang, W., Shi, G., Soon, W., Dodson, J., An, Z., 2019. Temperature seasonality and ENSO variability in the northern South China Sea during the Medieval Climate Anomaly interval derived from the Sr/Ca ratios of *Tridacna* shell. *Journal of Asian Earth Sciences* **180**, 103880. https://doi.org/10.1016/j.jseaes.2019.103880.

Marcott, S.A., Shakun, J.D., Clark, P.U., Mix, A.C., 2013. A reconstruction of regional and global temperature for the past 11,300 years. *Science* **339**, 1198–1201.

Ma, Y., Zhang, H., Pachur, H.-J., Wünnemann, B., Li, J., Feng, Z., 2004. Modern pollen-based interpretations of mid-Holocene palaeoclimate (8500 to 3000 cal. BP) at the southern margin of the Tengger Desert, northwestern China. *The Holocene* **14**, 841–850.

McCulloch, M., Mortimer, G., Esat, T., Li, X., Pillans, B., Chappell, J., 1996. High resolution windows into early Holocene climate: SrCa coral records from the Huon Peninsula. *Earth and Planetary Science Letters* **138**, 169–178.

McCulloch, M.T., Gagan, M.K., Mortimer, G.E., Chivas, A.R., Isdale, P.J., 1994. A high-resolution Sr/Ca and $\delta^{18}O$ coral record from the Great Barrier Reef, Australia, and the 1982–1983 El Nino. *Geochimica et Cosmochimica Acta* **58**, 2747–2754.

Paillard, D., Labeyrie, L., Yiou, P., 1996. Macintosh Program performs time-series analysis. *Eos* **77**, 379.

Petit, J.R., Jouzel, J., Raynaud, D., Barkov, N.I., Barnola, J.M., Basile, I., Bender, M., *et al.*, 1999. Climate and atmospheric history of the past 420,000 years from the Vostok ice core, Antarctica. *Nature* **399**, 429–436.

Polyak, V.J., Cokendolpher, J.C., Norton, R.A., Asmerom, Y., 2001. Wetter and cooler late Holocene climate in the southwestern United States from mites preserved in stalagmites. *Geology* **29**, 643–646.

Ren, X., Sha, Y., Shi, Z., Liu, X., 2021. Response of summer extreme precipitation over East Asia during the mid-Holocene versus future global warming. *Global and Planetary Change* **197**, 103398. https://doi.org/10.1016/j.gloplacha.2020.103398.

Roig, F.A., Le-Quesne, C., Boninsegna, J.A., Briffa, K.R., Lara, A., Grudd, H., Jones, P.D., Villagrán, C., 2001. Climate variability 50,000 years ago in mid-latitude Chile as reconstructed from tree rings. *Nature* **410**, 567–570.

Rosewater, J., 1964. The Family Tridacnidae in the Indo-Pacific. *Indo-Pacific Mollusca* **1**, 327–394.

Schöne, B.R., Pfeiffer, M., Pohlmann, T., Siegismund, F., 2005. A seasonally resolved bottom-water temperature record for the period AD 1866–2002 based on shells of *Arctica islandica* (Mollusca, North Sea). *International Journal of Climatology* **25**, 947–962.

Shao, D., Mei, Y., Yang, Z., Wang, Y., Yang, W., Gao, Y., Yang, L., Sun, L., 2020. Holocene ENSO variability in the South China Sea recorded by high-resolution oxygen isotope records from the shells of *Tridacna* spp. *Nature Scientific Reports* **10**, 3921. https://doi.org/10.1038/s41598-020-61013-2.

Shao, D., Yan, H., Wang, Y., Sun, L., 2012. High resolution Sr/Ca profiles of three *Tridacna* specimens and their potential as sea surface temperature proxy. *Journal of University of Science and Technology of China* **42**, 1–9.

Southon, J., Kashgarian, M., Fontugne, M., Metivier, B., W-S Yim, W., 2002. Marine reservoir corrections for the Indian Ocean and Southeast Asia. *Radiocarbon* **44**, 167–180.

Sun, D., Gagan, M.K., Cheng, H., Scott-Gagan, H., Dykoski, C.A., Edwards, R.L., Sua, R.X., 2005. Seasonal and interannual variability of the

https://doi.org/10.1017/qua.2021.28 Published online by Cambridge University Press

Mid-Holocene East Asian monsoon in $\delta^{18}O$ coral records from the South China Sea. *Earth and Planetary Science Letters* **237**, 69–84.

Tian, Q., Gou, X., Zhang, Y., Peng, J., Wang, J., Chen, T., 2007. Tree-ring based drought reconstruction (A.D. 1855–2001) for the Qilian Mountains, northwestern China. *Tree-Ring Research* **63**, 27–36.

Versteegh, E.A.A., Vonhof, H.B., Troelstra, S.R., Kaandorp, R.J.G., Kroon, D., 2010. Seasonally resolved growth of freshwater bivalves determined by oxygen and carbon isotope shell chemistry. *Geochemistry, Geophysics, Geosystems* **11**, Q08022. https://doi.org/10.1029/2009GC002961.

Wanamaker, A.D., Kreutz, K.J., Schöne, B.R., Introne, D.S., 2011. Gulf of Maine shells reveal changes in seawater temperature seasonality during the Medieval Climate Anomaly and the Little Ice Age. *Palaeogeography, Palaeoclimatology, Palaeoecology* **302**, 43–51.

Wang, H., He, S., 2012. Weakening relationship between East Asian winter monsoon and ENSO after mid-1970s. *Chinese Science Bulletin* **57**, 3535–3540.

Watanabe, T., Oba, T., 1999. Daily reconstruction of water temperature from oxygen isotopic ratios of a modern *Tridacna* shell using a freezing microtome sampling technique. *Journal of Geophysical Research* **104**, 20667–20674.

Watanabe, T., Suzuki, A., Kawahata, H., Kan, H., Ogawa, S., 2004. A 60-year isotopic record from a mid-Holocene fossil giant clam (*Tridacna gigas*) in the Ryukyu Islands: physiological and paleoclimatic implications. *Palaeogeography, Palaeoclimatology, Palaeoecology* **212**, 343–354.

Wei, G., Deng, W., Yu, K., Li, X., Sun, W., Zhao, J., 2007. Sea surface temperature records in the northern South China Sea from mid-Holocene coral Sr/Ca ratios. *Paleoceanography* **22**, PA3206. https://doi.org/10.1029/2006PA001270.

Wei, G., Sun, M., Li, X., Nie, B., 2000. Mg/Ca, Sr/Ca and U/Ca ratios of a *Porites* coral from Sanya Bay, Hainan Island, South China Sea and their relationships to sea surface temperature. *Palaeogeography, Palaeoclimatology, Palaeoecology* **162**, 59–74.

Wei, G., Yu, K., Zhao, J., 2004. Sea surface temperature variations recorded on coralline Sr/Ca ratios during Mid-Late Holocene in Leizhou Peninsula. *Chinese Science Bulletin* **49**, 1876–1881.

Welsh, K., Elliot, M., Tudhope, A., Ayling, B., Chappell, J., 2011. Giant bivalves (*Tridacna gigas*) as recorders of ENSO variability. *Earth and Planetary Science Letters* **307**, 266–270.

Winter, N.J., Vellekoop, J., Clark, A.J., Stassen, P., Speijer, R.P., Claeys, P., 2020. The giant marine gastropod *Campanile giganteum* (Lamarck, 1804) as a high-resolution archive of seasonality in the Eocene greenhouse world. *Geochemistry, Geophysics, Geosystems* **21**, e2019GC008794. https://doi.org/10.1029/2019GC008794.

Xu, X., Trumbore, S.E., Zheng, S., Southon, J.R., McDuffee, K.E., Luttgen, M., Liu, J.C., 2007. Modifying a sealed tube zinc reduction method for preparation of AMS graphite targets: reducing background and attaining high precision. *Nuclear Instruments and Methods in Physics Research Section B: Beam Interactions with Materials and Atoms* **259**, 320–329.

Yancheva, G., Nowaczyk, N.R., Mingram, J., Dulski, P., Schettler, G., Negendank, J.F., Liu, J., Sigman, D.M., Peterson, L.C., Haug, G.H., 2007. Influence of the intertropical convergence zone on the East Asian monsoon. *Nature* **445**, 74–77.

Yan, H., Liu, C., An, Z., Yang, W., Yang, Y., Huang, P., Qiu, S., *et al.*, 2020. Extreme weather events recorded by daily to hourly resolution biogeochemical proxies of marine giant clam shells. *Proceedings of the National Academy of Sciences of the United States of America* **117**, 7038–7043.

Yan, H., Liu, C., Zhang, W., Li, M., Zheng, X., Wei, G., Xie, L., Deng, W., Sun, L., 2017. ENSO variability around 2000 years ago recorded by *Tridacna gigas* $\delta^{18}O$ from the South China Sea. *Quaternary International* **452**, 148–154.

Yan, H., Shao, D., Wang, Y., Sun, L., 2013. Sr/Ca profile of long-lived *Tridacna gigas* bivalves from South China Sea: A new high-resolution SST proxy. *Geochimica et Cosmochimica Acta* **112**, 52–65.

Yan, H., Shao, D., Wang, Y., Sun, L., 2014a. Sr/Ca differences within and among three Tridacnidae species from the South China Sea: Implication for paleoclimate reconstruction. *Chemical Geology* **390**, 22–31.

Yan, H., Sun, L., Shao, D., Wang, Y., 2015. Seawater temperature seasonality in the South China Sea during the Late Holocene derived from high-resolution Sr/Ca ratios of *Tridacna gigas*. *Quaternary Research* **83**, 298–306.

Yan, H., Sun, L., Shao, D., Wang, Y., Wei, G., 2014b. Higher sea surface temperature in the northern South China Sea during the natural warm periods of late Holocene than recent decades. *Chinese Science Bulletin* **59**, 4115–4122.

Yan, H., Wang, Y., Sun, L., 2014c. High resolution oxygen isotope and grayscale records of a medieval fossil giant clam (*Tridacna gigas*) in the South China Sea: physiological and paleoclimatic implications. *Acta Oceanologica Sinica* **33**, 18–25.

Yu, K., Zhao, J., Wei, G., Cheng, X., Chen, T., Felis, T., Wang, P., Liu, T., 2005b. $\delta^{18}O$, Sr/Ca and Mg/Ca records of *Porites lutea* corals from Leizhou Peninsula, northern South China Sea, and their applicability as paleoclimatic indicators. *Palaeogeography, Palaeoclimatology, Palaeoecology* **218**, 57–73.

Yu, K., Zhao, J., Wei, G., Cheng, X., Wang, P., 2005a. Mid–late Holocene monsoon climate retrieved from seasonal Sr/Ca and $\delta^{18}O$ records of *Porites lutea* corals at Leizhou Peninsula, northern coast of South China Sea. *Global and Planetary Change* **47**, 301–316.

Zaw, Z., Fan, Z.X., Bräuning, A., Xu, C.X., Liu, W.J., Gaire, N.P., Panthi, S., Than, K.Z., 2020. Drought reconstruction over the past two centuries in southern Myanmar using Teak tree-rings: linkages to the Pacific and Indian oceans. *Geophysical Research Letters* **47**, e2020GL087627. https://doi.org/10.1029/2020GL087627.

Zhang, Y., Zhu, K., Huang, C., Kong, D., He, Y., Wang, H., Liu, W., Xie, Z., Wei, G., Liu, Z., 2019. Asian winter monsoon imprint on Holocene SST changes at the northern coast of the South China Sea. *Geophysical Research Letters* **46**, 13363–13370.

Zheng, X.F., Li, A.C., Wan, S.M., Jiang, F.Q., Kao, S.J., Johnson, C., 2014. ITCZ and ENSO pacing on East Asian winter monsoon variation during the Holocene: Sedimentological evidence from the Okinawa Trough. *Journal of Geophysical Research* **119**, 4410–4429.

https://doi.org/10.1017/qua.2021.28 Published online by Cambridge University Press